ChemPubSoc Europe

DOI: 10.1002/chem.201702665

CHEMISTRY
A European Journal
Full Paper

Boranes

In-Situ and Real-time Monitoring of Mechanochemical Preparation of $Li_2Mg(NH_2BH_3)_4$ and $Na_2Mg(NH_2BH_3)_4$ and Their Thermal Dehydrogenation

Nikola Biliškov,*[a] Andreas Borgschulte,[b] Krunoslav Užarević,[a] Ivan Halasz,[a] Stipe Lukin,[a] Sanja Milošević,[c] Igor Milanović,[a, c] and Jasmina Grbović Novaković[c]

Abstract: ■■Please add academic titles for authors■■For the first time, in situ monitoring of uninterrupted mechanochemical synthesis of two bimetallic amidoboranes, $M_2Mg(NH_2BH_3)_4$ (M = Li, Na), by means of Raman spectroscopy, has been applied. This approach allowed real-time observation of key intermediate phases, and a straightforward follow-up of the reaction course. Detailed analysis of time-dependent spectra revealed a two-step mechanism through $MNH_2BH_3{\cdot}NH_3BH_3$ adducts as key intermediate phases which further reacted with MgH_2, giving $M_2Mg(NH_2BH_3)_4$ as final products. The intermediates partially take a competitive pathway toward the oligomeric $M(BH_3NH_2BH_2NH_2BH_3)$ phases. The crystal structure of the novel bimetallic amidoborane $Li_2Mg(NH_2BH_3)_4$ was solved from high-resolution powder diffraction data and showed an analogous metal coordination to $Na_2Mg(NH_2BH_3)_4$, but a significantly different crystal packing. $Li_2Mg(NH_2BH_3)_4$ thermally dehydrogenates releasing highly pure H_2 in the amount of 7 wt.%, and at a lower temperature then its sodium analogue, making it significantly more viable for practical applications.

Introduction

In an attempt to find suitable materials for on-board solid state hydrogen storage, significant efforts are put towards ammonia borane (NH_3BH_3, AB), owing to its high gravimetric and volumetric hydrogen content (19.6 wt.% and 145 g dm^{-3}, respectively), as well as good stability under ambient conditions.[1] However, practical applications of AB for hydrogen storage are hindered by unfavorable reaction kinetics, along with the formation of gaseous ammonia and borazine as side-products of thermal dehydrogenation.[2,3] To improve the thermal behavior of solid AB, three main strategic approaches are employed: restriction of particles size to nanodimensions,[3–6] addition of catalytically active species,[7–9] and chemical modification.[10–14] Beneficial influence of any of these actions usually overcomes their obvious shortcoming, which is the reduction of hydrogen content relative to pristine AB.

Amidoboranes are a class of compounds derived from substitution of protic hydrogen on the N atom of AB with a metal ion; most often a light alkali or alkaline-earth metal.[12] It has been demonstrated by both experimental and theoretical studies that dehydrogenation performance of amidoboranes strongly depends on the ionicity and the size of the involved metal cation. Various metal species, having different atomic radii, charge, electronegativity, and coordination number, form bonding interactions with the $(NH_2BH_3)^-$ group, enabling tailoring of relevant properties, especially when more than one metal is involved.[15–19]

Several bimetallic amidoboranes of different stoichiometries were prepared by mechanical ball milling.[17–22] Although synthesis by ball milling is attractive due to its efficiency, often evidenced by quantitative and fast reactions occurring in a single step,[23] conducting mechanochemical reactions in closed and oscillating reaction vessels usually prohibited reaction optimization due to the inability to monitor its course without interrupting the milling process.[24] Consequently, these reactions were usually treated as black-box techniques and were conducted under tentatively chosen conditions. Resorting to ex situ reaction monitoring, where milling is periodically interrupted for sampling of the reaction mixture, is cumbersome, especially in the case of air- and moisture-sensitive hydride materials.

Therefore, the use of in situ and real-time monitoring would be of great help to overcome the aforementioned problems.

[a] N. Biliškov, K. Užarević, I. Halasz, S. Lukin, I. Milanović
Ruđer Bošković Institute
Bijenička c. 54, 10000 Zagreb (Croatia)
E-mail: nbilis@irb.hr

[b] A. Borgschulte
Swiss Federal Institute for Materials Science and Technology (EMPA)
Überlandstrasse 129, Dübendorf (Switzerland)

[c] S. Milošević, I. Milanović, J. G. Novaković
University of Belgrade, Vinča Institute of Nuclear Sciences
Laboratory for Material Sciences
PO Box 522, 11001 Belgrade (Serbia)

Supporting information including Rietveld fits of the XRD patterns of DSMAB and DLMAB; structure parameters; 2D representations of in situ Raman spectra of ball milling preparations; DSC and TPD-MS profiles; list of schools and high school students who contributed in mechanochemical preparations of the samples and the ORCID identification number(s) for the author(s) of this article can be found under: https://doi.org/10.1002/chem.201702665.

Recently, powder X-ray diffraction (PXRD)[25–27] and Raman spectroscopy[28–30] were introduced to study mechanochemical reactions in situ and in real time. Both methods have shown highly dynamic reaction environments, fast transformations, and formation of new phases.[31] The two techniques are complementary and can be employed simultaneously,[32] in order to understand the reactions pathways in details. While PXRD is suitable for monitoring of the evolution of bulk crystalline phases, Raman spectroscopy is more appropriate for monitoring of amorphous phases that are developed inside the mechanochemical reaction vessel. Moreover, in situ Raman spectroscopy is an affordable laboratory technique, unlike in situ PXRD, which requires access to a synchrotron radiation source.[27]

In our previous work, we thoroughly studied thermal dehydrogenation of AB by means of IR spectroscopy.[11] Here, we apply Raman spectroscopy to monitor mechanochemical synthesis of bimetallic amidoboranes of the general composition $M_2Mg(AB)_4$ (M = Na, Li, (AB) = NH_2BH_3) in situ and in real time. As a reference system, we took the previously reported $Na_2Mg(AB)_4$ (DSMAB),[13,17] to compare its properties and preparation with the novel $Li_2Mg(AB)_4$ (DLMAB).

To the best of our knowledge, this is the first in situ monitoring of mechanochemical synthesis of materials for solid-state hydrogen storage. Thus far, mechanisms of mechanochemical preparations of materials for solid-state hydrogen storage were mainly deduced from stepwise ex situ analysis, which provides only limited information due to an inherent time delay between sampling and analysis, but also due to the fact that sampling may irreproducibly disturb the mechanochemical process (different ball to powder ratio, exposure of the system to air etc.).[30,33]

On the other hand, by using in situ methods, evolution of the explored system can be monitored, including the formation and reactivity of any intermediate phases. Thus, the detailed preparation mechanism of two very prospective systems for solid-state hydrogen storage will be revealed in this work.

Experimental Section

Materials and synthesis

Ammonia borane, NH_3BH_3 (Sigma–Aldrich, technical grade, 90%) was used after recrystallization from diethyl ether, followed by a wash with ethanol.[34] Lithium hydride, LiH (Alfa Aesar, >97%), sodium hydride, NaH (Sigma–Aldrich, 95%) and magnesium hydride, MgH_2 (Sigma–Aldrich, hydrogen storage grade) was used as purchased. Handling of materials was carried out in an Ar filled MBraun LabMaster 1500 glove box, which ensures $\leq$0.1 ppm O_2 and H_2O, respectively.

Two types of mechanochemical reactors were used for the purposes of this study: 1) a Spex 8000M SamplePrep mill/shaker, equipped with hardened steel reaction jar; designed in-house and manufactured by Mitar Ltd and 2) an *iST*500 InSolido Technologies mill with poly(methyl methacrylate) (PMMA) ■■OK?■■ jars, designed and manufactured in-house. Stainless steel balls were used in both experiments. Equal products were obtained regardless of the setup used for milling.

The Spex 8000M was used for general preparations of the samples for further characterization. Stainless steel balls of the mass $m = 2\times4\text{ g} + 2\times1.7\text{ g}$ were used in these experiments. Milling frequency was 875 cycles per minute in a figure eight-shape motion, and the applied milling time was 30 min. In all preparations, the mass of reaction mixture was $\approx$250 mg.

The InSolido Technologies mill was used for all in situ monitoring experiments. The reactions were conducted in PMMA milling jars of 14 mL internal volume; transparent to the laser beam,[27] and two stainless steel balls of the mass $m = 4\text{ g} + 1.3\text{ g}$ were used. This mill applies linear back-and-forth movement geometry, with tunable frequency. We conducted the reactions at 30 Hz. Raman spectra were acquired by using an OceanOptics Maya2000Pro spectrometer, equipped with fiber optic probe and a 785 nm laser from PD-LD, USA for excitation. The setup has been previously published and thoroughly disclosed.[27,28] The experimental conditions, that is, lowered intensity of the laser beam (300 mW), in combination with rapid oscillations of the milling assembly and constant mixing of the reaction mixture, ensure negligible influence of laser radiation to reaction mixture. Spectral resolution is 4 cm^{-1}, which gives distance between subsequent points in the resulting spectrum $\Delta\tilde{\nu}$2 cm^{-1}. For each spectrum, 20 scans of 1 s were averaged, which gave $\Delta t = 20$ s time resolution.

Characterization

IR spectra were acquired in argon-filled glove box, using a Bruker Alpha spectrometer equipped with Platinum ATR accessory (single- reflection IIIa type diamond with 2×2 mm facet). The nominal resolution is 4 cm^{-1}, and each spectrum was taken as an average of 10 co-added Fourier-transformed interferograms (scans).

Raman spectra of samples DLMAB and DSMAB were recorded using a Bruker Senterra Raman microscope. As a source, the instrument uses a 532 nm laser. Spectral resolution was set to 5 cm^{-1}, while spatial resolution was <5 μm.

X-ray powder diffractograms (XRD) of the samples in a $\phi =$ 1 mm capillary were recorded at 30 °C using a Bruker D8 Advance diffractometer with Cu anode. The 2θ range was 10–90° with a $\Delta(2\theta) = 0.0221°$ step and counting time per step was 492.02 ms. Simulated annealing for structure solution was run until a plausible structure was found, where Mg atoms were found coordinated by four N atoms and Li atoms coordinated by hydrogen atoms of the BH_3 moiety. The structure model was refined using the Rietveld method, together with unit cell parameters, coefficients of the shifted Chebyshev polynomial used to describe background, peak position, and shape parameters. All structure solution and refinement calculations were performed using the program Topas.[35] CCDC 432929 (DLMAB) contains the supplementary crystallographic data for this paper. These data are provided free of charge by The Cambridge Crystallographic Data Centre.

Thermogravimetric and differential thermal analysis (TG/DTA) was performed simultaneously with a Mettler Toledo TA 4000

system. Measurements were done under N_2 flow at a rate of 50 mL min^{-1}, in the 25–200 °C range. Heating rate was 2 °C min^{-1}.

The differential scanning calorimetry (DSC) measurements were conducted with a SETARAM DSC131 evo device. Measurements were done in temperature range from 30 to 200 °C, with heating rate of 2 °C min^{-1}, under constant N_2 flow. Enthalpies of solid-state phase changes are calculated from areas under Lorentzian functions, fitted to individual thermal events of DSC profiles. From these areas, enthalpy change of the first and second dehydrogenation are obtained using the equation [Eq. (1)]:

$$\Delta H = \frac{MS_{peak}}{\beta} \quad (1)$$

where M is molar mass of initial compound in g mol^{-1}, S_{peak} is the area under the DSC peak in kW s^{-1}, and β is ramping rate in K s^{-1}.

To analyze the composition of gaseous products (EGA) of thermal dehydrogenation of samples, a home-made setup for temperature programmed desorption (TPD), coupled with an Extorr 3000 quadrupole mass spectrometer (MS) was used. It uses up to 5 mg of powdered sample in a quartz tube, placed inside an electrical furnace. Prior to measurement, the tube with sample was outgassed at room temperature and 10^{-7} torr. After that, the sample was linearly heated at 10 °C min^{-1} from room temperature to 200 °C. The EGA signals, as partial pressures, at 8 different m/z ratios were followed and simultaneously recorded as a function of temperature. The observed m/z ratios were: 1 (H), 2 (H_2), 17 (NH_3 or OH), 18 (H_2O), 28 (B_2H_6), 43 (μ-$(NH_2)B_2H_5$), 58 (cyclo-$(NH_2BH_2)_2$), 81 (cyclo-$(NHBH)_3$).

Results and Discussion

Preparation of $M_2Mg(AB)_4$

Mechanochemical preparation of $Na_2Mg(AB)_4$ (DSMAB) using a planetary mill, directly from the corresponding stoichiometric mixture of NaH, MgH_2, and AB was previously reported.[17] Since we use a high-energy mill-shaker for ball milling reactions, we checked the applicability of this mill to repeat the reported reaction. Both IR spectra and XRD patterns (Figure 1) confirm that this synthesis was successfully repeated. This allows the application of the same conditions to obtain the $Li_2Mg(AB)_4$ (DLMAB). The general chemical reaction of the preparation of $M_2Mg(AB)_4$ is [Eq. (2)]:

$$2\,MH + MgH_2 + 4\,NH_3BH_3 \rightarrow M_2Mg(NH_2BH_3)_4 + 4\,H_2 \quad (2)$$

where M = Li or Na. 30 min milling of the stoichiometric mixture of LiH, MgH_2, and AB resulted in a product. The similarity of IR and Raman spectra of obtained product with those for DSMAB (Figure 1, Table 1) indicates the successfully prepared DLMAB.

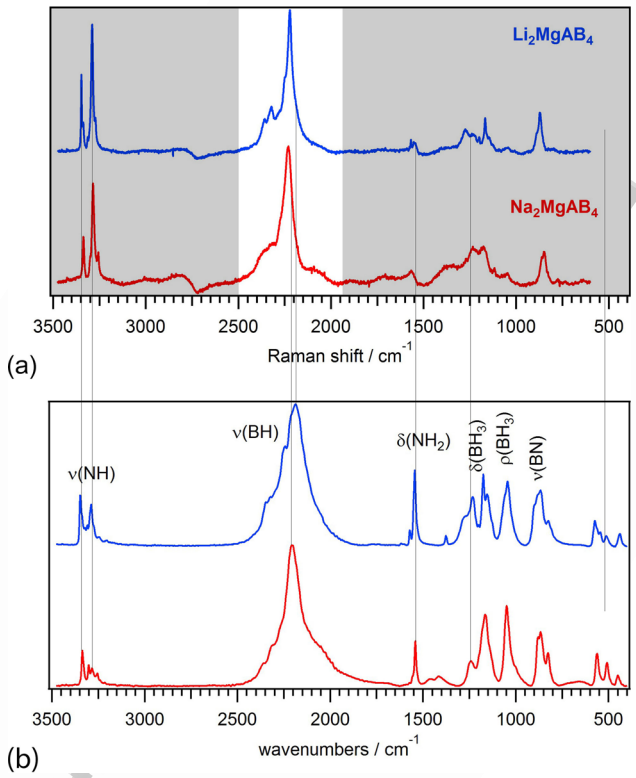

Figure 1. Comparison of DLMAB and DSMAB: (a) Raman spectra (white field denotes the observed spectral window around ν(BH) envelope); (b) IR spectra with approximate assignation.

Table 1. IR and Raman spectra of DLMAB and DSMAB. Units: cm^{-1}

DLMAB		DSMAB		
IR	Raman	IR	Raman	Assignment[a]
3346 s	3347 s	3335 s	3336 s	ν_{as}(NH)
3337 w	3338 m			
3321 w	3314 m			
3309 w		3301 m		ν_{as}(NH)[b]
3288 s	3290 vs	3284 m	3285 vs	ν_s(NH)
3273 w	3272 m	3256 w	3256 m	ν_s(NH)[b]
2346 w	2358 w	2359 w	2358 w	ν_{as}(BH)[b]
2322 w	2322 m	2313 w	2322 w	ν_{as}(BH)
2244 m	2249 m	2267 w		
2186 s	2222 vs	2205 vs	2230 vs	ν_s(BH)
1570 w	1568 m	1556 w	1566 m	δ_{as}(NH_2)
1544 s	1544 m	1541 m		
1375 w	1370 w	1415 w	1370 w	
1275 w	1275 m			
1232 m	1235 w	1241 m	1235 m	δ_s(NH_2)
	1168 m	1164 m	1188 w	δ_{as}(BH_3)
1152 m	146 w	1153 w	1126 w	δ_s(BH_3)
1044 m	1048 w	1049 m	1047 w	ρ(NH_3)
899 m	891 w			
880 m	872 m	880 m	849 m	ν(BN)
825 w		826 w		
574 w		562 w		
545 w				
512 w		509 w		
438 w		449 w		

[a] According to Ref. [11] [b] Degradation products, Ref. [36].

Structure and composition

Although DSMAB and DLMAB have very similar IR and Raman spectra, their XRD patterns are very different. (Figure 1). This indicates that crystallographically they are not isostructural, although M and Mg atoms are equally coordinated in both systems (Figure 1).

The diffraction pattern of DLMAB was indexed using an orthorhombic unit cell, which left several peaks unindexed. The quality of the Pawley fit, however, suggested that these may be due to impurities. Parts of the pattern with major impurity peaks were at first excluded. The crystal structure of DLMAB was solved in direct space by simulated annealing, taking the amidoborane moiety as a rigid body. The Li and Mg atoms were treated as independent atoms.

Rietveld fitting of the powder XRD for DLMAB (Figure 2) shows that it crystallizes in the orthorhombic *Pbcn* space group with one lithium atom, two AB moieties, and 1/2 of Mg atom comprising the asymmetric unit; satisfying the overall charge neutrality. The Mg atom lies on the second order axis (Wyckoff position *c* in the *Pbcn* space group). In DLMAB, analogous to DSMAB,[17] magnesium is tetrahedrally coordinated by nitrogen atoms of the amido groups while lithium is coordinated by hydrogen atoms of the BH_3 moiety, in a distorted coordination environment (Figure 3). Thus, coordination of metal atoms in DLMAB is analogous to that in DSMAB. However, packing is significantly different in these two systems.

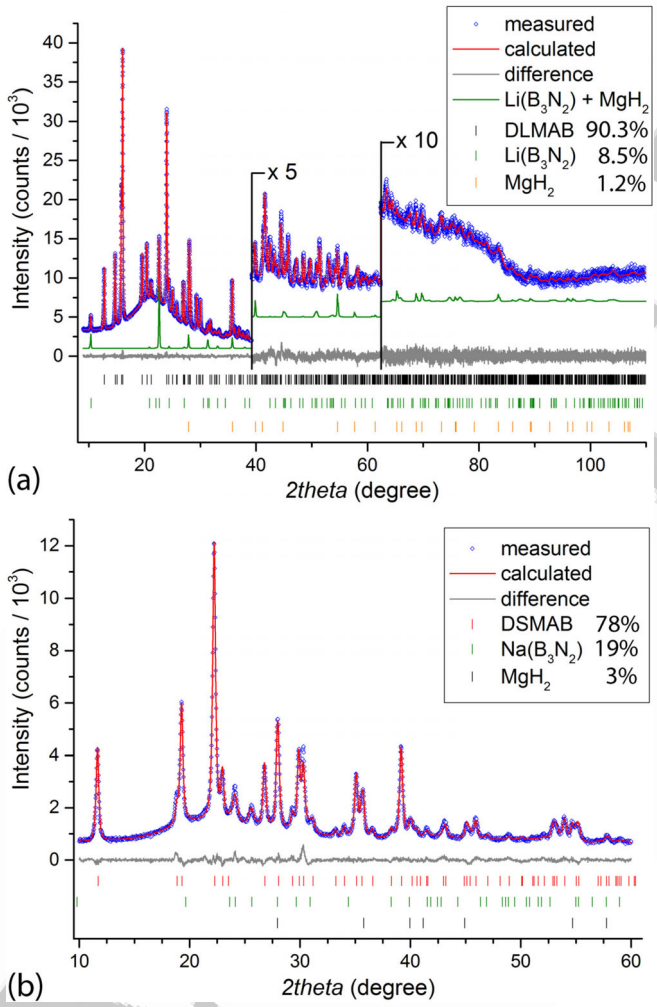

Figure 2. Quantitative composition of DLMAB and DSMAB samples, as determined from powder XRD patterns by fitting the patterns for (a) DLMAB and (b) DSMAB to MgH_2[37] and $M(B_3N_2)$.[36] For analysis of DSMAB, $Na_2Mg(AB)_4$ was taken from ref. [17], while the structure of $Li_2Mg(AB)_4$ was solved by Rietveld refinement.

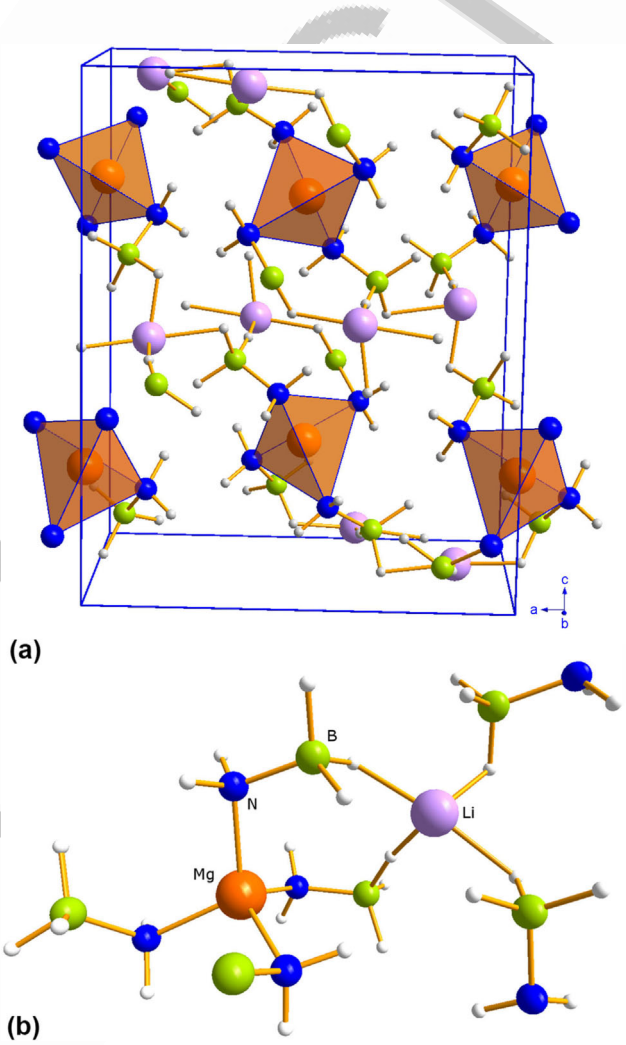

Figure 3. (a) Crystal packing and (b) bonding environment of DLMAB. Each Mg^{2+} is bound to four N^- forming a tetrahedron with $NH_2BH_3^-$ groups, and each Li^+ is octahedrally coordinated through six hydride H atoms of $NH_2BH_3^-$ moieties.

This is further consolidated by Rietveld analysis (Figure 2), which shows that diffractograms for both DLMAB and DSMAB are fully described by a predominant $M_2Mg(AB)_4$ phase, with a contribution of long-chain $M(BH_3NH_2BH_2NH_2BH_3)$ (further denoted in the text as the $M(B_3N_2)$) phase[36] and MgH_2[37] (Figure 2). Attribution of diffraction patterns for both DLMAB and DSMAB to these three-phase systems provided an excellent fit to the experimental data (Figures 2 and Figures S1–S3 in Supporting Information). The appearance of $Na(B_3N_2)$ phase during mechanochemical synthesis has been already report-

ed.[17] Even more interesting, $Na_2Mg(AB)_4$, as prepared in THF solution from NaH, $Mg(NH_2)_2$, and AB, also contains this phase.[13] Practically the equal intensity ratio of XRD peaks for sample prepared by ball milling with respect of that prepared in solution indicates that the equal mechanism takes place irrespective of the preparation method.[13,17]

Mechanistic considerations

In order to reveal the reaction pathway through which amidoboranes are prepared by milling, as well as the emergence and development of observed $M(B_3N_2)$ species, we used Raman spectroscopy to monitor ball milling reactions in situ (Figures S4 and S5). Unfortunately, the intensity of the overall spectra is relatively low, allowing only the ν(BH) region to be accurately analyzed. First, a strong band due to the PMMA reaction vessel in the 3200–2650 cm^{-1} range completely overlaps the ν(NH) region (see the Supporting Information for an illustrative example). On the other hand, the bands lying in the fingerprint region are of low intensity, disabling accurate intensity measurements. Thus, further considerations are based exclusively on measurements of the ν(BH) envelope by fitting it to appropriate Lorentzian profile functions.

The spectrum of $2\,NaH + MgH_2 + 4\,AB$ reaction, as taken at $t = 0$ min, differs from AB in a significant reduction of overall intensity, as well as appearance of a prominent feature at 2188 cm^{-1} and weak bands at 2103 and 2067 cm^{-1}. This undoubtedly shows that a new phase is produced immediately when NaH come into contact with AB. The molar ratio of the reactants (NaH:AB = 1:2), comparison with available spectra, as well as the behavior of the $2\,LiH + MgH_2 + 4\,AB$ system, altogether indicates that an intermediate species of $NaNH_2BH_3{\cdot}NH_3BH_3$ (Na(AB)·AB) composition is produced at this stage (Figure 4). In these spectra, the clear 2315 cm^{-1} band of Na(AB)·AB is represented as a shoulder, which is explainable by the lower resolution of in situ spectra, as well as the band broadening due to the dynamic conditions in which the spectra are acquired. At best of our knowledge, Na(AB)·AB is not yet reported, but a detailed description of this species is out of the scope of the present paper.

The initial reaction of AB with LiH is significantly slower with respect to NaH. The spectrum, as taken at $t = 0$ min, shows that the reaction mixture consists of intact reagents AB, LiH, and MgH_2 (Figure 5). In the first 10 min of milling an intermediate phase is produced (Figures 5 and 6b). This phase is represented in Raman spectra with 2368 and 2325 cm^{-1} bands, as well as a broad shoulder at 2195 cm^{-1}, with preservation of a strong 2281 cm^{-1} band. Figure S6, shows evolution of the position of the ν_{as}(BH) band. It clearly shows that, although the development of new bands is evident (Figure 5), this particular vibration is not significantly affected by the initial reaction. The molar ratio of LiH and AB, as well as low reactivity of MgH_2 with AB, indicates the formation of a $LiNH_2BH_3{\cdot}NH_3BH_3$ intermediate phase (further in the text Li(AB)·AB) at this stage. In order to check this hypothesis, we reproduced the previously reported synthesis of the Li(AB)·AB adduct.[38] Comparison of XRD patterns (Supporting Information) proves this route. Thus,

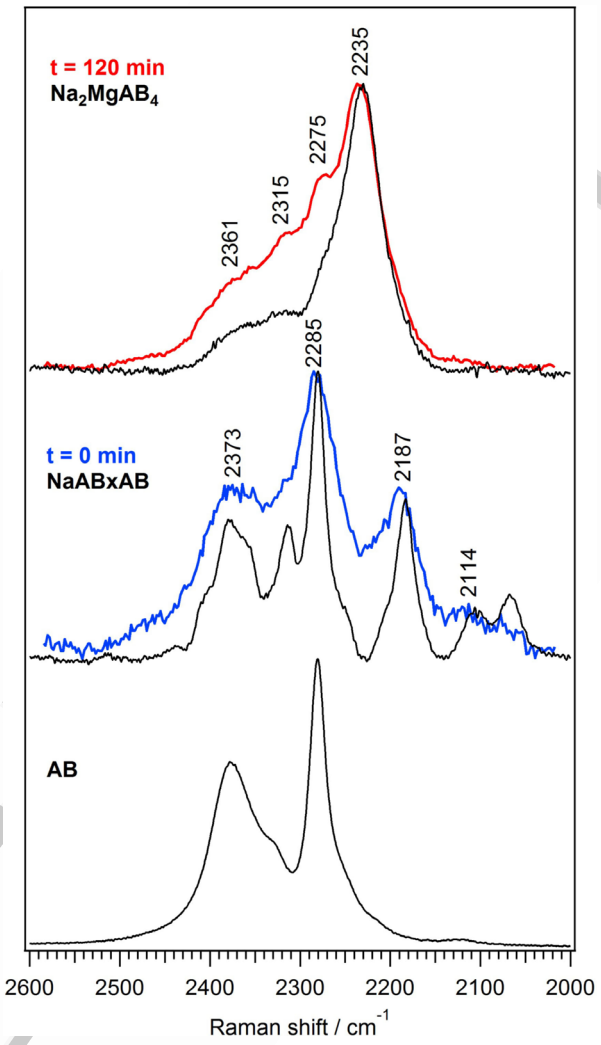

Figure 4. Representative Raman spectrum of the initial stage of reaction $2\,NaH + MgH_2 + 4\,AB$ and its comparison with AB and Na(AB)·AB spectra.

the following reaction represents the first step in the production of intermediate $M_2Mg(AB)_4$ (M = Li or Na) [Eq. (3)]:

$$MH + 2\,AB \xrightarrow{B.M.} M(AB) \cdot AB_{(s)} + H_2(g) \qquad (3)$$

The intensities of the spectral features attributed to the M(AB)·AB phases suffer a steep decrease, simultaneously with an increase of new features (Figures 4 and 5). The most characteristic band for both species appears at 2230 cm^{-1} and this is used to follow the evolution of the product (black dots in Figure 6). However, at this stage the ν_{as}(BH) band (Figure S6) shifts toward the lower wavenumbers, reflecting a significant weakening of the B–H bond due to the reaction of M(AB)·AB with MgH_2. Indeed, structural parameters (Table S1 in Supporting Information) show a significantly longer B–H band in $M_2Mg(AB)_4$ systems with respect to AB. Thus, the intermediate species, produced according to Equation (3), are a prerequisite for further reaction with MgH_2, giving the final product $M_2Mg(AB)_4$ [Eq. (4)]:

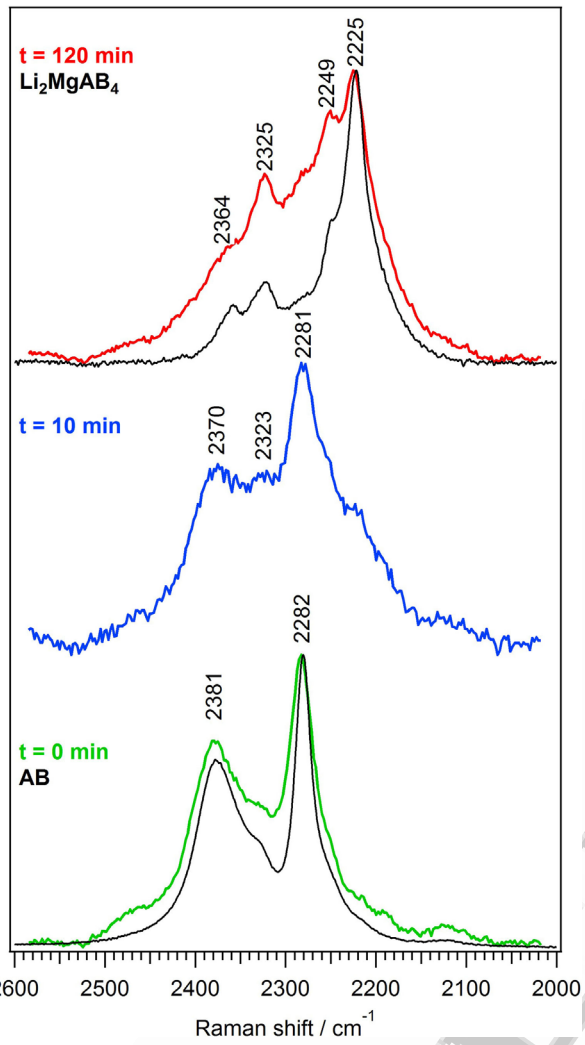

Figure 5. Representative Raman spectra as taken during the milling of $2\,LiH + MgH_2 + 4\,AB$ mixture and their comparison with AB and DLMAB.

$$2\,M(AB)\cdot AB + MgH_2 \xrightarrow{B.M.} M_2Mg(AB)_{4(s)} + 2\,H_2(g) \quad (4)$$

This reaction takes place simultaneously with formation of the M(AB)·AB intermediate phase, and it includes substitution of M^+ with Mg^{2+}, forming Mg–N bonds with coordination of Li^+ or Na^+ with BH groups through hydride hydrogens.

In both cases, a significant drop of intensities of all the spectral features is observed, which reflects gluing of the reaction mixture (green lines in Figure 6). After some time, the spectra reappear. This behavior indicates formation of a Mg-containing intermediate phases. On the basis of available experimental data we cannot deduce the composition of this intermediate phase. At this stage we can only speculate about complexation of Mg^{2+} (or MgH_2) with M(AB)·AB. These instable species readily rearrange into the final $M_2Mg(AB)_4$. This hypothesis seems reasonable, since, according to the molecular structures of DSMAB[17] and DLMAB (Figure 3) with respect of Li(AB) and Na(AB),[10] Mg^{2+} substitutes for M^+ and is covalently bonded with the N of AB and extrudes it to coordinate with the BH moiety. However, the confirmation of this hypothesis, as well as elucidation of the structure of this intermediate, is out of scope of the present study.

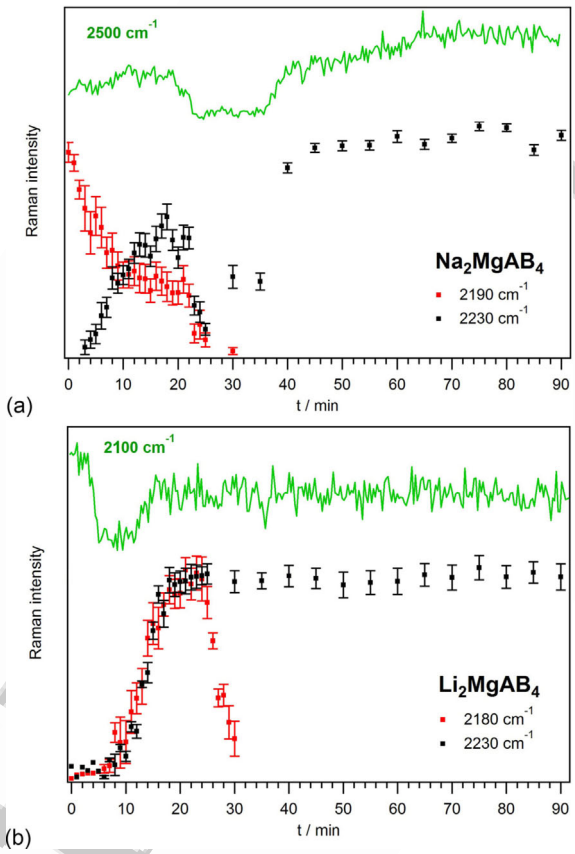

Figure 6. Temporal evolution of the M(AB)·AB and $M_2Mg(AB)_4$ species (2230 cm^{-1}) species as measured during the preparation of (a) DSMAB and (b) DLMAB by fitting the Raman band at (2190 cm^{-1}) and (2230 cm^{-1}), respectively, to Lorentzian profile function. Intensities, as shown here, are not in range. Green curves represents the behavior of the low-intensity feature at 2500 cm^{-1} for DSMAB and at 2100 cm^{-1} for DLMAB, indicating the gluing of the reaction mixture to the vessel during the milling.

In both cases, after the reappearance of the spectra, the intensity of the 2230 cm^{-1} band reaches the plateau (Figure 6). After this step, no further spectral changes are observed, indicating formation of the final products, and consequent termination of the reactions. In order to check this, the IR spectrum and XRD of the sample DSMAB after 90 min of milling, were compared with those previously published,[17] which confirms formation of $Na_2Mg(AB)_4$, as well as $Li_2Mg(AB)_4$. Figure 6 also shows that the reaction of MgH_2 with Li(AB)·AB is $\approx 1.5\times$ faster than with Na(AB)·AB, as determined by fitting of the linear part of the $I(2230\ cm^{-1}) = f(t)$ and the duration of the "sticky" intermediate phase, in accordance with the evidence of generally higher reactivity of Li-containing compounds.[39]

The presence of $M(B_3N_2)$ is confirmed by analysis of powder XRD (see Figure 2 for DLMAB).[36,40] Also, Raman spectra show that the features attributable to $M(B_3N_2)$ species arise soon after the start of mechanochemical synthesis, following the production of M(AB)·AB, and these features persist over the rest of the reaction. This shows that the reaction of M(AB)·AB with MgH_2 (Eq. 4) is in competition with [Eq. (5)]:

$$M(AB)\cdot AB + AB \xrightarrow{\Delta} M(B_3N_2)_{(s)} + NH_3(g) + H_2(g) \quad (5)$$

The presence of NH_3 in reaction vessels at the end of the reaction further supports this interpretation. Eventually the excess AB is completely consumed by reaction (5), which proceeds in the first phase of the synthesis, and this process is in competition with reaction that include MgH_2, giving rise to DLMAB.

Let us consider the observation that the $Na(B_3N_2)$ phase is produced regardless of the reaction conditions, that is, it is observed in the same amount from XRD of DSMAB prepared from THF solution of NaH, MgH_2, and AB[13] and by ball milling,[17] as repeated here. This strongly indicates the same mechanistic pathway, which is independent of reaction medium. In this reaction, THF acts exclusively as a solvent which does not affect the reaction by itself. In the other words, it only enables molecular mobility, which is the driving force of the reaction, in the same way as transfer of energy by balls in the mechanochemical approach. In both cases, Na(AB)·AB is produced by reaction (3) in the first step, and the formed intermediate phase further reacts through (4) giving the $Na_2Mg(AB)_4$ as a dominant product. However, the side reaction (5) is also evident in both cases, resulting in $Na(B_3N_2)$. Although the absolute rate of first and second step of this reaction can vary with respect of reaction conditions, the ratio of rates of reactions involved in the second step is insensitive to applied conditions.

Thermal dehydrogenation

TG reveals a two-step H_2 release from DSMAB[17] at 137 and 171 °C and in a minor extent at 85 °C at 2 °C min^{-1} heating rate. In the case of DLMAB, a small loss of the mass around 85 °C is observed. As seen from comparison of TPD with the derivative of TG for DLMAB (Figure 7), TG is well correlated with emission of H_2, confirming that its thermal decomposition is accompanied by release of hydrogen as a predominant gaseous product.

Phase transformations of $M_2Mg(AB)_4$ from room temperature to 200 °C were followed by DSC (Figure 7). DSMAB shows several distinct features: an endothermic process in the temperature range 40–70 °C with a maximum at 60 °C, followed by three exothermic processes as listed in Table 2 and shown in Figures S7 and S8. The endothermic reaction preceding thermal decomposition is characteristic for Na and Li amidoboranes.[41] The weak endothermic DSC peak can be attributed to melting or amorphization of the mixture,[42] eventually yielding species containing $M(NH_3)^+$ cations.[41] Here the suggested synthetic route leads to formation of a Li-containing system with DSC profile given in Figure 7. The observed exothermic processes occur at lower temperatures than those for pure AB[11] and AB/MgH_2 mixture.[43] In contrast to results of Nakagawa et al.,[42] who have observed three exothermic peaks at 53, 117, and 131 °C in AB/$LiAlH_4$ system, DSC analysis of DLMAB sample reveals two additional processes at 80 and 151 °C.

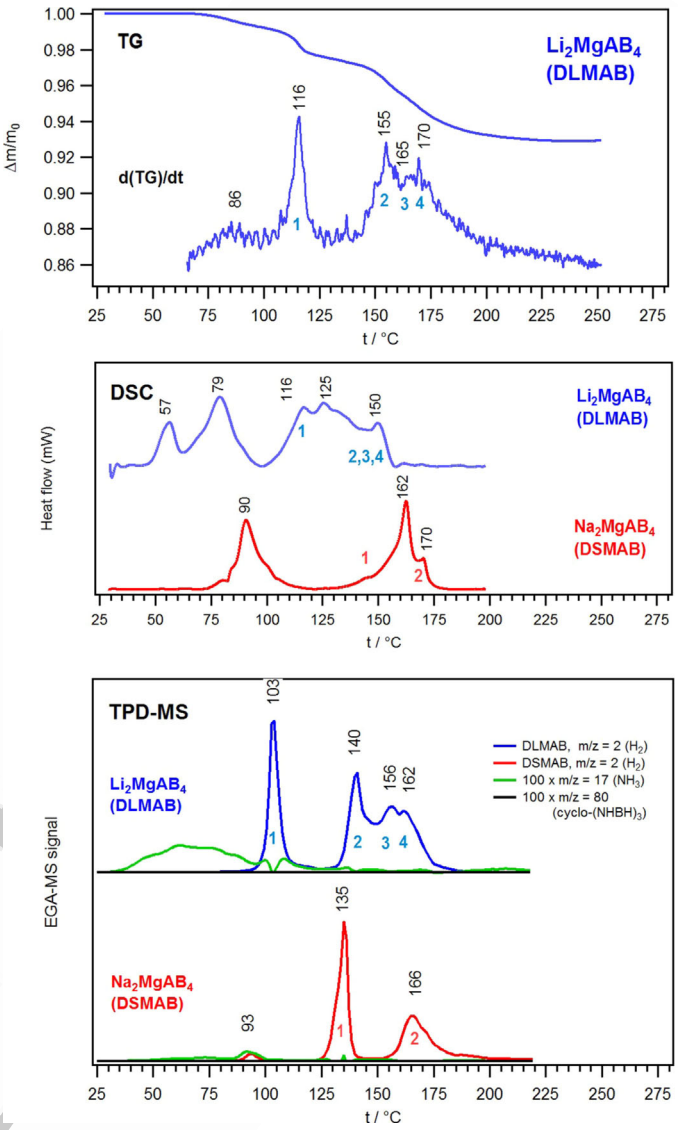

Figure 7. The TG, DSC, and TPD-MS ($m/z = 2$ (H_2), 17 (NH_3, intensity multiplied by 100) and 81 ($(NHBH)_3$, intensity multiplied by 100) profiles for thermal decomposition of DLMAB and DSMAB. The individual H_2 desorption events are numbered.

The obvious difference in TPD-MS and DSC curves is due to the difference in thermodynamic driving force,[44,45] that is, experimental conditions. DSMAB (Figure 7 and Table 2) shows three desorption maxima. TPD-MS analysis shows that hydrogen is generated as a consequence of both high-temperature chemical conversions. The process taking place at 93 °C is accompanied by NH_3 emission. In both DLMAB and DSMAB cases, NH_3 is released in amount of <1% in total gas, which is consistent with calculated very high deammoniation energies with respect to those for dehydrogenation.[19] However, DLMAB releases somewhat more NH_3 with respect to DSMAB, which is also consistent with the observed trends. In the 130–180 °C region, three maxima (Table 2, Figures S9 and S10) are observed, in accordance with previously published results.[46] At this stage, we can assume that this is caused by formation of $M(B_3N_2)$ phase. Although this species is undoubtedly ob-

Table 2. Temperatures of DSC and TPD-MS peaks, enthalpies of chemical transformations that result in release of H_2 (calculated from areas below Gaussian profiles fitted to DSC curve), and quantity of released hydrogen as calculated from area under H_2 temperature desorption maxima, fitted to Lorentzian profiles.

DSMAB				DLMAB			
DSC		TPD		DSC		TPD	
t [°C]	ΔH [kJ mol^{-1}]	t [°C]	% H_2	t [°C]	ΔH [kJ mol^{-1}]	t [°C]	% H_2
thermal event not observed				56		60	0[a]
91	39.4 ± 0.5[b]	93	3	78		80	0[a]
146		135	27	116	30.1 ± 0.1[c]	103	29
162	48.4 ± 0.7[d]	–	–	126		–	–
170		166	22	150	29.9 ± 0.7[e]	160[f]	39

[a] Exclusively NH_3 detected by TPD-MS (Figure 7). [b] 1st dehydrogenation step for DSMAB (TPD event at 93 °C). [c] 1st dehydrogenation step for DLMAB (TPD event at 103 °C). [d] 2nd dehydrogenation step for DSMAB (TPD events in the 135–166 °C range). [e] 2nd dehydrogenation step for DLMAB (TPD events in the 140–160 °C range). [f] Sum of 156 and 162 °C feature (Figure 7).

served in our material, further studies are required to confirm this hypothesis.

At the current stage, our observations and measured dehydrogenation energies (Table 2) are consistent with dehydrogenation mechanism for bimetallic Mg-containing amidoboranes as proposed and computationally analyzed.[15,19,47] In other words, the decomposition mechanism involves intermolecular production of H_2 through alkaline hydride-mediated oligomerization of the neighboring $[NH_2BH_3]^-$ groups by $BH^{\delta-}\cdots{}^{+\delta}HN$ dihydrogen bonding interaction. The hydride H^- from BH_3 groups of $[NH_2BH_3]^-$ moiety is transferred to Na^+ or Li^+ forming alkaline hydride MH, which subsequently interacts with the protic H^+ of the $Mg(NH_2BH_3)^{2-}$ group. H is released as a consequence of this reaction. Since the formation of a new B–N bond is an exothermic process, whereas bond breaking is an endothermic process, it results in relatively small total value of dehydrogenation ΔH.

Conclusions

The present results provide a new entry for a systematic understanding and rational control of mechanochemical preparation of systems for solid-state hydrogen storage. The novel mixed-metal amidoborane $Li_2Mg(AB)_4$ (DLMAB) has been prepared by direct ball milling of the reaction mixture ($2\,LiH + MgH_2 + 4\,AB$), in a similar way to its Na-containing analogue (DSMAB). The crystal structure of DLMAB was determined from powder XRD and refined using the Rietveld method. Coordination of metal atoms is equal to that for DSMAB, that is, each Mg^{2+} is tetrahedrally coordinated with N atoms of NH_2BH_3 moieties, while Li^+ forms distorted octahedra through 6 Li-H-B coordination bonds. Although bonding and coordination are similar for the two systems, crystal packing of DLMAB significantly differs from DSMAB.

To the best of our knowledge, in situ Raman spectroscopy is here for the first time employed for uninterrupted, real-time monitoring of mechanochemical preparation of hydrogen storage materials. For both DLMAB and DSMAB, a two-step reaction pathway is revealed, where LiH or NaH first react with AB, giving intermediate M(AB)·AB species. In the second step, it reacts with MgH_2, giving $M_2Mg(AB)_4$. However, this second step is in competition with a side-reaction leading to $M(BH_3NH_2BH_2NH_2BH_3)$, resulting in a moderate contamination of the final products. This byproduct phase is produced irrespective of reaction conditions. It is demonstrated that DLMAB releases pure H_2 in the 7 wt.% amount, with trace amounts of NH_3 and B_2H_6 contamination, and no detectable borazine. Although the detailed desorption mechanism of both phases is still unknown and needs to be further investigated in detail, the results are highly consistent with previously proposed mechanism that involves intermolecular oligomerization through the interaction of neighboring $NH_2BH_3^-$ groups. At this stage we can conclude that DLMAB would be a potential candidate for PEM fuel cell vehicle applications.

Acknowledgements

This work was supported by the Ministry of Environment and Energy, the Ministry of Science and Education, the Environmental Protection and Energy Efficiency Fund and the Croatian Science Foundation under the project "New Materials for Energy Storage", in the total amount of 1962100.00 HRK, and by MEST of Serbia under grant III45012. It arose in the framework of the Serbian–Croatian bilateral project "Ammonia Borane and Its Derivatives for Solid-State Hydrogen Storage", and a part of this work was realized in the framework of the COST Action MP1103 "Nanostructured materials for solid-state hydrogen storage". We are indebted to Mr. Vitomir Stanišić and his team from the workshop of the Ruđer Bošković Institute for their continuous support. N.B. wishes to thank Foundation "Knowledge in Action", which enabled a workshop for high school students of several high schools from Zagreb in his laboratory (list of schools and students is given in Supporting Information). We are grateful to Zoran Jovanovic' for TPD measurements.

Conflict of interest

The authors declare no conflict of interest.

Keywords: amidoboranes · hydrogen storage · mechanochemistry · Raman spectroscopy · Thermal dehydrogenation

[1] J.-H. Luo, X.-D. Kang, P. Wang, *J. Phys. Chem. C* **2010**, *114*, 10606–10611.
[2] P. F. Yuan, F. Wang, Q. Sun, Y. Jia, Z. X. Guo, *Int. J. Hydrogen Energy* **2013**, *38*, 11313–11320.
[3] A. Gutowska, L. Li, Y. Shin, C. M. Wang, X. S. Li, J. C. Linehan, R. S. Smith, B. D. Kay, B. Schmid, W. Shaw, M. Gutowski, T. Autrey, *Angew. Chem. Int. Ed.* **2005**, *44*, 3578–3582; *Angew. Chem.* **2005**, *117*, 3644–3648.
[4] M. E. Bluhm, M. G. Bradley, R. Butterick III, U. Kusari, L. G. Sneddon, *J. Am. Chem. Soc.* **2006**, *128*, 7748–7749.

[5] A. Feaver, S. Sepehri, P. Shamberger, A. Stowe, T. Autrey, G. Cao, *J. Phys. Chem. B* **2007**, *111*, 7469 – 7472.
[6] D. Neiner, A. Luedtke, A. Karkamkar, W. Shaw, J. Wang, N. D. Browning, T. Autrey, S. M. Kauzlarich, *J. Phys. Chem. C* **2010**, *114*, 13935 – 13941.
[7] F. H. Stephens, V. Pons, R. T. Baker, *Dalton Trans.* **2007**, 2613 – 2626.
[8] M. C. Denney, V. Pons, T. J. Hebden, D. M. Heinekey, K. I. Goldberg, *J. Am. Chem. Soc.* **2006**, *128*, 12048 – 12049.
[9] R. J. Keaton, J. M. Blacquiere, R. T. Baker, *J. Am. Chem. Soc.* **2007**, *129*, 1844 – 1845.
[10] Z. Xiong, C. K. Yong, G. Wu, P. Chen, W. Shaw, A. Karkamkar, T. Autrey, M. O. Jones, S. R. Johnson, P. P. Edwards, W. I. F. David, *Nat. Mater.* **2008**, *7*, 138 – 141.
[11] N. Biliškov, D. Vojta, L. Kótai, I. M. Szilágyi, D. Hunyadi, T. Pasinszki, T. Flinčec Grgac, S. Borgschulte, A. Züttel, *J. Phys. Chem. C* **2016**, *120*, 25276 – 25288.
[12] Y. S. Chua, P. Chen, G. Wu, Z. Xiong, *Chem. Commun.* **2011**, *47*, 5116 – 5129.
[13] Y. S. Chua, W. Li, G. Wu, Z. Xiong, P. Chen, *Chem. Mater.* **2012**, *24*, 3574 – 3581.
[14] A. Staubitz, A. P. M. Robertson, I. Manners, *Chem. Rev.* **2010**, *110*, 4079 – 4124.
[15] D. Y. Kim, H. M. Lee, J. Seo, S. K. Shin, K. S. Kim, *Phys. Chem. Chem. Phys.* **2010**, *12*, 5446 – 5453.
[16] A. T. Luedtke, T. Autrey, *Inorg. Chem.* **2010**, *49*, 3905 – 3910.
[17] H. Wu, W. Zhou, F. E. Pinkerton, M. S. Meyer, Q. Yao, S. Gadipelli, T. J. Udovic, T. Yildirim, J. J. Rush, *Chem. Commun.* **2011**, *47*, 4102 – 4104.
[18] R. Owarzany, P. J. Leszczynski, K. J. Fijalkowski, W. Grochala, *Crystals* **2016**, *6*, 88.
[19] K. Wang, J. G. Zhang, T. Li, Y. Liu, T. Zhang, Z. N. Zhou, *Int. J. Hydrogen Energy* **2015**, *40*, 2500 – 2508.
[20] X. Kang, J. Luo, Q. Zhang, P. Wang, *Dalton Trans.* **2011**, *40*, 3799 – 3801.
[21] X. Kang, H. Wu, J. Luo, W. Zhou, P. Wang, *J. Mater. Chem.* **2012**, *22*, 13174 – 13179.
[22] Y. S. Chua, H. Wu, W. Zhou, T. J. Udovic, G. Wu, Z. Xiong, M. W. Wong, P. Chen, *Inorg. Chem.* **2012**, *51*, 1599 – 1603.
[23] S. L. James, et al., *Chem. Soc. Rev.* **2012**, *41*, 413 – 447.
[24] I. A. Tumanov, A. F. Achkasov, E. V. Boldyreva, V. V. Boldyrev, *CrystEngComm* **2011**, *13*, 2213 – 2216.
[25] T. Friščić, I. Halasz, P. A. Beldon, A. M. Belenguer, F. Adams, S. A. J. Kimber, V. Honkimäki, R. E. Dinnebier, *Nat. Chem.* **2013**, *5*, 66 – 73.
[26] I. Halasz, A. Puškarić, S. A. J. Kimber, P. J. Beldon, A. M. Belenguer, F. Adams, V. Honkimäki, R. E. Dinnebier, B. Patel, W. Jones, V. Štrukil, T. Friščić, *Angew. Chem. Int. Ed.* **2013**, *52*, 11538 – 11541; *Angew. Chem.* **2013**, *125*, 11752 – 11755.
[27] I. Halasz, S. A. J. Kimber, P. J. Beldon, A. M. Belenguer, F. Adams, V. Honkimäki, R. C. Nightingale, R. E. Dinnebier, T. Friščić, *Nat. Protoc.* **2013**, *8*, 1718 – 1729.
[28] D. Gracin, V. Štrukil, T. Friščić, I. Halasz, K. Užarević, *Angew. Chem. Int. Ed.* **2014**, *53*, 6193 – 6197; *Angew. Chem.* **2014**, *126*, 6307 – 6311.
[29] M. Juribašić, K. Užarević, D. Gracin, M. Ćurić, *Chem. Commun.* **2014**, *50*, 10287 – 10290.
[30] M. Tireli, M. Juribašić Kulcsar, N. Cindro, D. Gracin, N. Biliškov, M. Borovina, M. Ćurić, I. Halasz, K. Užarević, *Chem. Commun.* **2015**, *51*, 8058 – 8061.
[31] A. D. Katsenis, A. Puškarić, V. Štrukil, C. Mottillo, P. A. Julien, M. H. Užarević, K. Pham, T. O. Do, S. A. J. Kimber, P. Lazić, O. Magdysyuk, R. E. Dinnebier, I. Halasz, T. Friščić, *Nat. Commun.* **2015**, *6*, 6662.
[32] L. Batzdorf, F. Fischer, M. Wilke, K. J. Wenzel, F. Emmerling, *Angew. Chem. Int. Ed.* **2015**, *54*, 1799 – 1802; *Angew. Chem.* **2015**, *127*, 1819 – 1822.
[33] S. Kurko, L. Matović, N. Novaković, B. Matović, Z. Jovanović, B. Paskaš Mamula, J. Grbović Novaković, *Int. J. Hydrogen Energy* **2011**, *36*, 1184 – 1189.
[34] T. Autrey, A. Gutowska, L. Li, J. Linehan, M. Gutowski, *Prepr. Symp. Am. Chem. Soc. Div. Fuel Chem.* **2004**, *49*, 150 – 151.
[35] Bruker-AXS, (2009) Topas version 4.2.
[36] K. J. Fijalkowski, T. Jaron, P. J. Leszczynski, E. Magos-Palasyuk, T. Palasyuk, M. K. Cyranski, W. Grochala, *Phys. Chem. Chem. Phys.* **2014**, *16*, 23340 – 23346.
[37] T. Moriwaki, Y. Akahama, H. Kawamura, S. Nakano, K. Takemura, *J. Phys. Soc. Jpn.* **2006**, *75*, 074603.
[38] C. Wu, G. Wu, Z. Xiong, W. I. F. David, K. R. Ryan, M. O. Jones, P. P. Edwards, H. Chu, P. Chen, *Inorg. Chem.* **2010**, *49*, 4319 – 4323.
[39] I. Dovgaliuk, L. H. Jepsen, D. A. Safin, Z. Łodziana, V. Dyadkin, T. R. Jensen, M. Devillers, Y. Filinchuk, *Chem. Eur. J.* **2015**, *21*, 14562 – 14570.
[40] R. Owarzany, K. J. Fijalkowski, T. Jaroń, P. J. Leszczyński, L. Dobrzycki, M. K. Cyrański, W. Grochala, *Inorg. Chem.* **2016**, *55*, 37 – 45.
[41] K. J. Fijalkowski, R. V. Genova, Y. Filinchuk, A. Budzianowski, M. Derzsi, T. Jaroń, P. J. Leszczynski, W. Grochala, *Dalton Trans.* **2011**, *40*, 4407 – 4413.
[42] Y. Nakagawa, K. Shinzato, T. Nakagawa, K. Nakajima, S. Isobe, K. Goshome, H. Miyaoka, T. Ichikawa, *Int. J. Hydrogen Energy* **2016**, *42*, 6173 – 6180.
[43] X. Kang, L. Ma, Z. Fang, L. Gao, J. Luo, S. Wang, P. Wang, *Phys. Chem. Chem. Phys.* **2009**, *11*, 2507 – 2513.
[44] T. Durojaiye, A. Goudy, *Int. J. Hydrogen Energy* **2012**, *37*, 3298 – 3304.
[45] G. Pokol, *J. Therm. Anal. Calorim.* **2000**, *60*, 879 – 886.
[46] Y. Nakagawa, S. Isobe, Y. Ikarashi, S. Ohnuki, *J. Mater. Chem. A* **2014**, *2*, 3926 – 3931.
[47] K. Wang, J.-G. Zhang, *Chem. Phys. Lett.* **2013**, *590*, 27 – 34.

Manuscript received: June 9, 2017
Accepted manuscript online: September 13, 2017
Version of record online: ■■ ■■, 0000

FULL PAPER

Boranes

N. Biliškov, A. Borgschulte, K. Užarević, I. Halasz, S. Lukin, S. Milošević, I. Milanović, J. G. Novaković*

■■ – ■■

In-Situ and Real-time Monitoring of Mechanochemical Preparation of $Li_2Mg(NH_2BH_3)_4$ and $Na_2Mg(NH_2BH_3)_4$ and Their Thermal Dehydrogenation

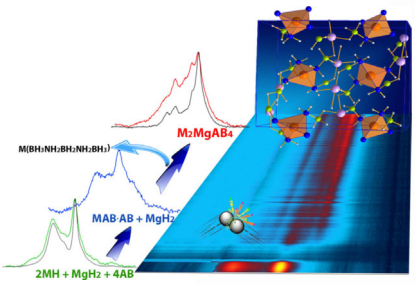

Have a ball: In situ monitoring of the mechanochemical synthesis of bimetallic amidoboranes allowed real-time observation of key intermediate phases, and a straightforward follow-up of the reaction course. The crystal structure of the novel bimetallic amidoborane $Li_2Mg(NH_2BH_3)_4$ was solved from powder diffraction data and showed an analogous metal coordination to $Na_2Mg(NH_2BH_3)_4$, but a significantly different crystal packing.

Biliškov et al. on in situ monitoring of mechanochemical synthesis @institutrb @Empa CH @Univerzitet BG
SPACE RESERVED FOR IMAGE AND LINK

Share your work on social media! *Chemistry - A European Journal* has added Twitter as a means to promote your article. Twitter is an online microblogging service that enables its users to send and read text-based messages of up to 140 characters, known as "tweets". Please check the pre-written tweet in the galley proofs for accuracy. Should you or your institute have a Twitter account, please let us know the appropriate username (i.e., @accountname), and we will do our best to include this information in the tweet. This tweet will be posted to the journal's Twitter account @ChemEurJ (follow us!) upon online publication of your article, and we recommended you to repost ("retweet") it to alert other researchers about your publication.

Please check that the ORCID identifiers listed below are correct. We encourage all authors to provide an ORCID identifier for each coauthor. ORCID is a registry that provides researchers with a unique digital identifier. Some funding agencies recommend or even require the inclusion of ORCID IDs in all published articles, and authors should consult their funding agency guidelines for details. Registration is easy and free; for further information, see http://orcid.org/.

Nikola Biliškov http://orcid.org/0000-0002-6981-944X
Andreas Borgschulte http://orcid.org/0000-0001-6250-4667
Krunoslav Užarević http://orcid.org/0000-0002-7513-6485
Ivan Halasz
Stipe Lukin http://orcid.org/0000-0003-2247-6803
Sanja Milošević
Igor Milanović
Jasmina Grbović Novaković